PHYSICAL REVIEW B VOLUME 16, NUMBER 4 15 AUGUST 1977

Linearized secondary-electron cascades from the surfaces of metals. II. Surface and subsurface sources

E. N. Sickafus
Research Staff, Ford Motor Company, Dearborn, Michigan 48121
(Received 18 October 1976; revised manuscript received 11 March 1977)

Segmentation of the linearized cascade from a metallic surface was shown in Paper I to be initiated by internal sources. Here the nature of the line shape accompanying the segmentation is related to a distinction between internal sources according to surface and subsurface distributions of their constituents. These sources are assumed to be activated during the decay processes that accompany excitation of bound electrons by passing primary electrons and derive from atomic constituents having distinguishable spatial distributions. The distributions correspond to a surface source if they exist within an inelastic mean free path $l_i(E)$ of the vacuum-solid interface, and are subsurface sources if they exist below this level in the solid. Composite distributions are considered also. Characteristic spectra in the $\log j(E)/\log(E)$ display mode are shown for nitrogen, oxygen, carbon, and sulfur serving as internal sources in nickel and aluminum.

I. INTRODUCTION

In the preceding paper, which we will refer to as I, the linearization of the secondary-electron cascade associated with an external monoenergetic beam of electrons was discussed. The cascade was hypothesized ideally to have the form AE^{-m}. Although a simple model predicts a linear cascade in the $\log j(E)/\log(E)$ display mode, one observes linear segments which are associated with internal sources.[1] The segmentation is found to be bounded near energy values that correlate with core levels of the constituent atoms of the solid. In this paper, we take a detailed look at the regions joining the segments of a linearized cascade. Emphasis is placed on segmentation by Auger-electron sources and these are analyzed in terms of surface and subsurface sources. The surfaces of atomically characterized metals are examined in the energy region of 10–1000 eV corresponding to the shortest inelastic mean free paths for electrons.

In I it was demonstrated that the linearization of the cascade in the $\log j(E)/\log(E)$ display mode is consistent with the major features of cascade theory[2] in spite of some limitations. The theory assumes spherical scattering in the center-of-mass system and can accomodate only a homogeneous source. It predicts a homogeneous and isotropic distribution of internal secondary electrons. More complex source functions, of a type that would be conducive to realistic modeling of surface conditions, have not been found to be mathematically tractable as yet.[3] Thus, in dealing here with surface versus subsurface sources our analysis necessarily is based on a hypothetical model involving linear line shapes for the cascades resulting from internal and external sources. This hypothesis has been reached from many observations in several metallic systems.

In Sec. II, brief comments about experimental details are made. Details relating to specimen preparation and mounting are given in Paper I. In Sec. III, we present the line-shape hypothesis and other theoretical comments. Section IV contains the experimental findings and these are discussed in Sec. V.

II. EXPERIMENTAL DETAILS

Specimen preparation, mounting, and cleaning are discussed briefly in Sec. II of I. There it was mentioned that a clean surface is prerequiste to observing a linearized cascade. A "clean surface" refers to the ideal termination of a homogeneous solid; i.e., no adsorbates or segregated impurities. Here we are interested in observing the segmentation of the cascade associated with Auger electron sources in and near the surface. For clean surfaces and surfaces having a fractional monolayer coverage of another (or several) atomic species, this is a straightforward process. However, thick overlayers can distort completely the linearization of the cascade. The problem is particularly noticeable with carbon. The presence of carbon at the surface tends to cause strong attenuation of electron intensity in the cascade and in the case of large coverage causes curvature of the cascade at low energies, $E<275$ eV, in a sense similar to the escape probability effect (compare Figs. 1 and 2 of I). How much carbon is required for a given amount of cascade curvature, or electron attenuation, has not been evaluated.

The electronic circuitry used with our four-grid spherical sector, low-energy-electron diffraction (LEED) optics to obtain $\log j(E)/\log(E)$ displays is

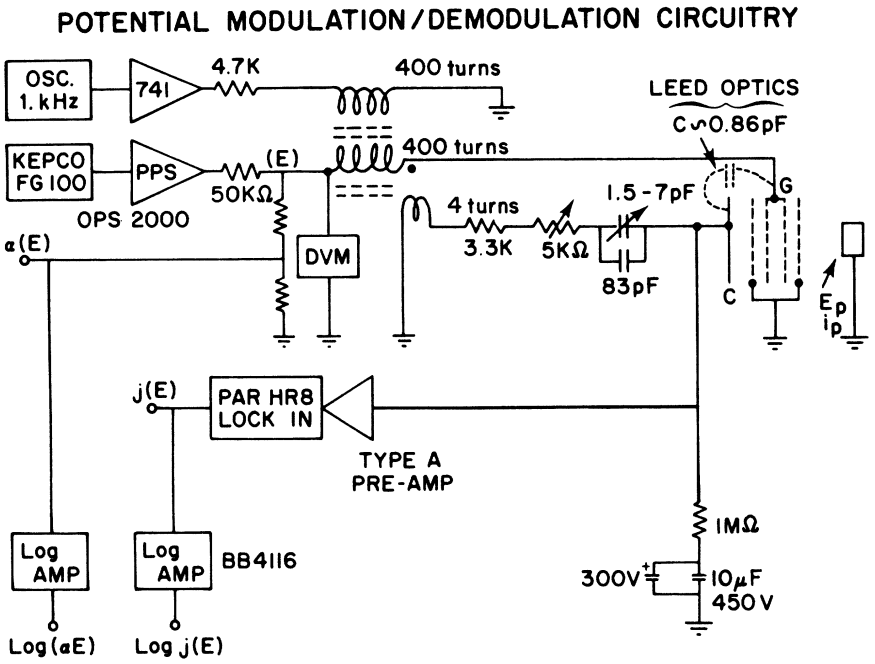

FIG. 1. Schematic wiring diagram of the electronic circuit used with hemispherical-sector LEED optics to energy-analyze secondary-electron emission. sion. The transformer portion of the circuit, along with the tunable capacitor is designed to balance capacitive coupling between the modulated retarding grids (*G*) and the collector (*C*). The LOCKIN amplifier is referenced externally to the 1-kHz oscillator. Analog signals are available before or after the logarithmic amplifiers depending on the signal desired. Circuit components are designated in the text.

shown schematically in Fig. 1. The transformer and tunable-capacitor circuitry coupling the retarding grids with the collector are designed to compensate for capacitive coupling between the retarding grids and the collector. The effective capacitance to be compensated is ~0.86 pF and is indicated by broken lines in the figure. The transformer was wound on two Series 3019 type 3B7 Ferroxcube pot cores using two 400-turn windings of No. 34 gauge copper wire and one four-turn winding of No. 28 gauge stranded copper wire to obtain an inductance of $L \sim 1.5$ H. The oscillator is a fixed-frequency Burr Brown 4023 operating at 1 kHz, the programmable power supply (PPS) is a Kepco OPS-2000 driven by a Kepco FG-100 function generator, and the logarithmic amplifiers are Burr Brown 4116. The dc level of the retarding potential is monitored with a digital volt meter and a proportional analog signal is obtained from a 1:1000 voltage divider. This signal is equated to the kinetic energy threshold of electrons reaching the collector with no correction for contact potential. The beam current is measured as the return current to ground of the accelerating-potential power supply.

III. THEORETICAL DISCUSSION

Analysis of the secondary-electron cascade based on the Boltzmann diffusion equation gives useful insight into a model involving a homogeneous source in a semi-infinite solid bounded by a planar surface (see I). No solution is known for an inhomogeneous solid. Thus, we are unable at the present time to present a theoretical analysis of secondary emission appropriate for surface and subsurface sources in the energy region of shortest inelastic mean free paths. Instead, a hypothesis is presented which characterizes line shapes in the cascade to be expected with surface and subsurface sources. A certain amount of justification for this hypothesis can be based on the existing cascade theory, the rest is based on numerous experimental studies of linearized cascades.

We separate ideally surface and subsurface sources by an energy-dependent boundary at a depth $l_i(E)$ from the surface, where $l_i(E)$ is the inelastic mean free path of an electron of energy E, see Fig. 2. Justification for this delineation is discussed later. Thus the model has two parts: (i) The subsurface region represented by a semi-infinite homogeneous solid bounded by a planar surface—the interface lying at a depth $l_i(E)$ from the actual vacuum solid interface and (ii) a homogeneous surface region having plane parallel surfaces and thickness $l_i(E)$, bounded on one side by the vacuum and on the other by the subsurface region. Three types of internal sources are considered: the first is a surface source, the second is a homogeneous subsurface source, and the third is a composite surface-subsurface, homogeneous source. These are illustrated in Fig. 2 along with their line shapes including their cascade regions.

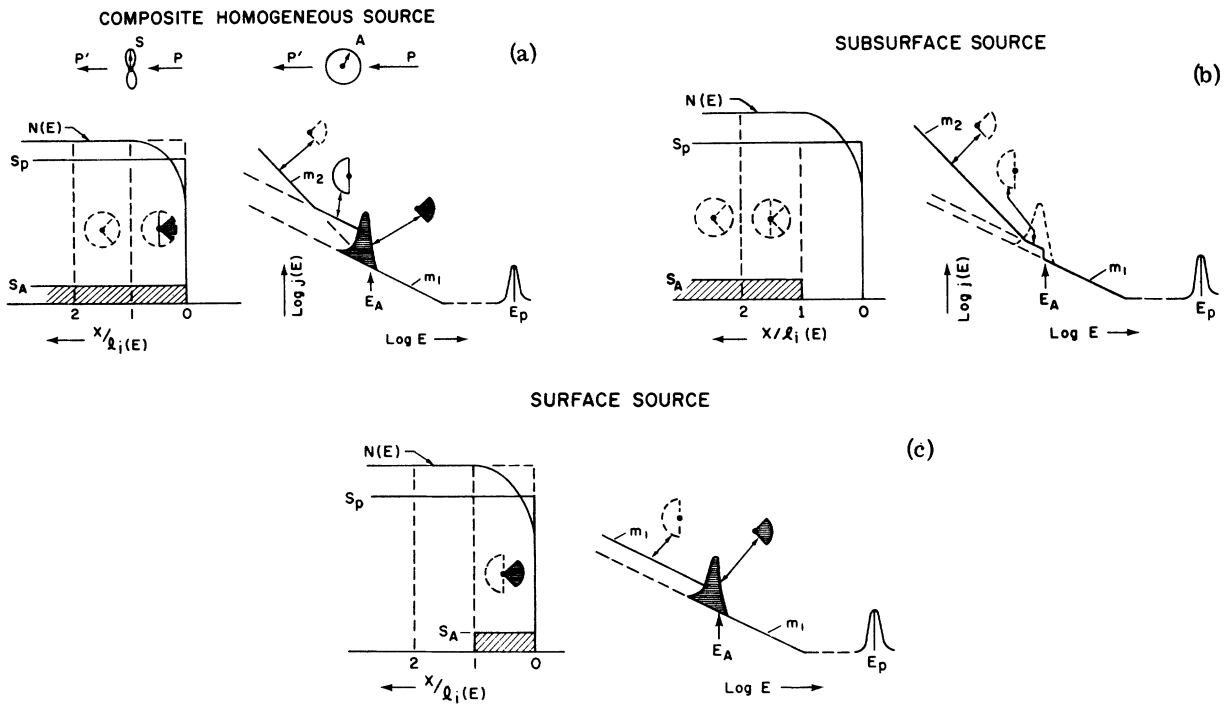

FIG. 2. (a) In the upper portion of this figure is illustrated the general difference in angular dependence of excitation of free electrons (S) by primaries ($P \rightarrow P'$) and bound electrons (A) by primaries ($P \rightarrow P'$). The former is more perpendicular to the path of the primary while the latter essentially is independent of the path of the primary. In the lower left-hand part of the figure is shown a comparison of the source-strength distributions associated with an external source S_P and an auxiliary, internal source S_A, along with the resultant cascade distribution function $N(E)$, for a composite homogenous source. To the right is shown the corresponding line shape in the $\log j(E)/\log(E)$ display mode near the characteristic energy threshold E_A of the auxiliary source. The line of slope m_1 represents the overall cascade associated with the primary beam, E_p. The shaded area of the circle represents characteristic emission from the auxiliary source in the surface region $0 \leq x/l_i(E) \leq 1$ that can escape elastically to produce a characteristic line shape, shown shaded in the $\log j(E)/\log(E)$ curve. The open half circle and broken-line sector designate electrons which give rise to (partially) thermalized cascade emission as illustrated. (b) Illustrated here is a subsurface auxiliary source corresponding to emission S_A from a source distributed in the solid below the surface region, $[x/l_i(E)] \geq 1$. A characteristic peak for the auxiliary source is missing since all of S_A is subject to inelastic scattering before any of it can escape through the surface. The parallel step of slope m_1 is largely attenuated since the contribution from the surface region is absent. There results, in effect, an enhanced second slope m_2. (c) Surface region distribution of an auxiliary internal source of strength S_A is illustrated along with its characteristic line shape following the threshold at E_A. The parallel step of m_1 is now the most prominent feature. (See text for details).

Each of these sources is assumed to be excited by ionization of bound electron states during passage through the solid of the incident primary beam and is therefore proportional in intensity to the primary beam intensity and the number of atoms according to an appropriate cross section (and, where required, a backscattering correction).

The terminology of internal and external sources is used here for convenience to distinguish between two types of distributed sources which produce similar types of excitations. "External source" is used to refer to the incident (external) primary beam which is able to cause excitations of the free electrons and, consequently, has an associated cascade. Due to its range, the primary beam is, in effect, a distributed source. When the primary beam has sufficient energy, it may cause ionization of bound electron states which give rise to Auger electron emission, and in effect, produces a new distributed "internal source." Such emission also is able to cause excitation of the free electrons and has an associated cascade. Internal sources can be excited by any internal electrons (or photons) having sufficient energy. The strengths of these sources are referred to herein as S_p corresponding to an external source and S_A corresponding to an internal source.

Consider first a composite homogeneous model (surface plus subsurface). An incident primary beam produces, in the steady state, a homogeneous distribution of internal secondaries $N(E', \beta)$, as described in I. Here, E' is the internal kinetic

energy of the electron measured relative to the bottom of the band, β is the angle between the electron's velocity vector and the inward surface normal, E is the external kinetic energy measured relative to the vacuum level, and α is the angle between the electron's velocity vector and the outward normal to the surface. The external current leaving the surface, $j(E,\alpha)$, is a direct sample of this distribution, resulting from electrons escaping the solid from depths weighted exponentially by $l_i(E)$. The cascade belonging to the primary beam (the external-source cascade) has a linear characteristic in the $\log j(E)/\log(E)$ display mode. To this model add an internal source (homogeneous) having a threshold energy E_A lying in the range of the external-source cascade. The effect, as derived in I, is to segment the resultant cascade near E_A producing a positive step with a net offset of the linear cascade parallel to itself. This follows because the sources (external and internal) are treated additively in the solution for $N(E',\beta)$; see Eq. (19) in I. This clearly is an incomplete picture because internal and external sources cannot have identical characteristics as is implied by adding their strengths. A fundamental difference is that internal sources near the surface can emit directly into (or toward) the half space containing the detector whereas primary electrons, because they are incident upon the surface, require more scattering events to return their electrons to the detector half space. On the other hand, the emission by an internal source into the half space of the specimen can be thought of as having a resultant cascade similar to that of an external source and describable by summing source intensities because both source contributions can be thought of as becoming equally "thermalized" with the lattice.

The emission by an internal source into the half space containing the detector can be expected to produce a cascade with a characteristic different from that of an external source. It will require fewer scattering events to bring these electrons to positions favorable for escape at the surface. Therefore, they are not as thermalized with the lattice as are the external-source cascade electrons and consequently do not result in a uniform increase in population of the thermalized current. Thus, whatever the cascade characteristic, it will be relatively more intense, compared with the thermalized component, at all energies below the threshold. We assume that this cascade characteristic also is linear in $\log j(E)/\log(E)$ but that its slope is added to that existing prior ($E > E_A$) to the threshold energy E_A.

The model of a composite homogeneous source is illustrated in Fig. 2(a). The left-hand part is a plot of source strengths, which are assumed to be proportional to concentration, for the host lattice, S_p, and for an additional internal source, S_A. The boundary $x/l_i = 1$ separates the surface-source region from the subsurface-source region. $N(E)$ is the internal distribution function. Since the theory was limited to a homogeneous source and no gradient of N was permitted, the distribution function is homogeneous also. However, we show in Fig. 2 a gradient of $N(E)$ in the surface region to emphasize that a part of the distribution in this region is lost by direct emission into the vacuum, which accounts for the detected current $j(E)$.

In addition to the (inelastic) cascade components (from S_A and S_p) the current leaving the surface can have a characteristic (elastic) component associated with the threshold E_A. Ignoring, for the moment, attenuation effects, a simple model demonstrates the extent of the source of characteristic emission. Direct (elastic) emission into the vacuum from within the surface region can occur at various angles so long as the internal path length does not exceed $l_i(E)$. Considering all possible angles of emission from colinear positions on the inward normal to the surface results in a volume bounded by a surface of revolution given by

$$[x/l_i(E)]^{2/3}+[y/l_i(E)]^{2/3}=1\,, \tag{1}$$

where x is measured along the inward normal and y lies in the planar interface, see Fig. 3. From this model, 23% of the emission from a surface

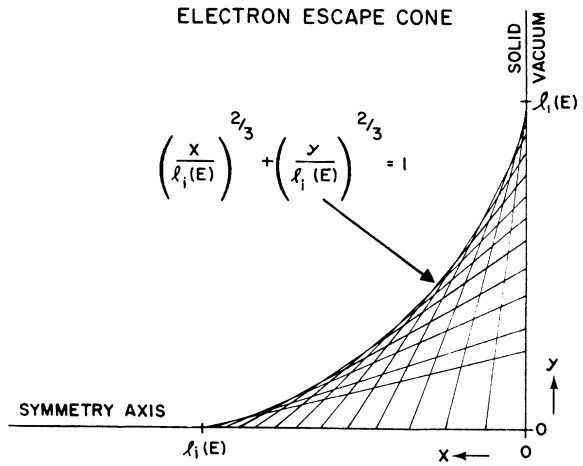

FIG. 3. Electron-escape cone characterizing the angular dependence of elastic emission subject to an internal path length $l_i(E)$—the inelastic mean free path. The x axis is directed along the inward normal to a planar surface in which is placed the y axis. The x axis is thus the axis of symmetry. Electrons originating along the x axis can escape through the surface provided that their velocities lie within this cone of revolution.

source can reach the surface elastically. This compares with a value of 21% when allowing exponential attenuation from infinite depths.

In the upper part of Fig. 2(a) is illustrated the angular dependence of secondaries generated from "free" electrons by primaries (the source S_p) and the angular dependence of Auger emission generated from bound electrons by primaries (the source S_A). When a high-speed primary P interacts with an essentially stationary, free electron of the solid it does so by a Coulomb interaction which imparts a perpendicular momentum[4] to the secondary S with little change in direction of the primary, P'. The Auger-type of internal source shown to the right is more isotropic, as indicated by the circle labeled A associated with the primary transition $P \rightarrow P'$. As shown in the source profile plot of Fig. 2(a), Auger emission within the surface region has a portion (shaded area of the circle) that escapes elastically into the vacuum. This is evidenced in a characteristic line, the Auger peak, as shown in the $\log j(E)/\log(E)$ plot in Fig. 2(a). Auger emission by the surface source into the subsurface region (the semicircle in the surface region) eventually becomes thermalized along with the cascade associated with the primaries and results in a step at $\log(E_A)$ with slope parallel to the prethreshold region, m_1. The remaining emission from the surface region that does not escape and the outward emission segment drawn in the second layer of Fig. 2(a) do not become equivalently thermalized and are an additive current contributing to the new slope m_2.

Illustrated in Fig. 2(b), is the subsurface source which is homogeneous in the source strength S_A while the source generated by primaries S_p is homogeneous throughout the composite structure. There is no Auger emission in the surface layer and thus an Auger peak is absent in $\log j(E)/\log(E)$. The parallel-slope step can be present, none the less, because the inward Auger emission can become thermalized along with the source S_A. However, if present, it is expected to be attenuated strongly due to the absence of any contribution from S_A in the surface region. The new slope m_2 develops because of outwardly directed emission from the subsurface region and is now the dominant feature.

The surface source is illustrated in Fig. 2(c) where the emission S_A exists only in the surface layer. Here the outward emission within the escape cone produces a characteristic Auger peak. The inward emission combines with S_P to produce the parallel-slope step, while the new slope m_2 either does not develop or is very weak because of the limited amount of forward emission that can appear as an independent current.

This model of segmented cascades is summarized as follows: A surface source has a prethreshold ($E > E_A$) cascade given by

$$\log j(E) = -m \log(E) + \log b, \quad E_A \leq E \leq E_{cp}. \tag{2}$$

At and near (below) the threshold it will have a line shape characteristic, for example, of elastic emission of Auger electrons plus "rediffused" Auger electrons. Following this characteristic line will be the cascade associated with the surface source having the same slope as the prethreshold region but offset parallel to it:

$$\log j(E) = -m \log(E) + \log b_A, \quad E \leq E_A \tag{3}$$

where the difference in the constants $\log b_A$ and $\log b$ is related to the strength of the surface source S_A [see Eq. (19) I]. Emission from a subsurface source will have a change of slope in the cascade near the threshold so that

$$\log j(E) = -m_A \log(E) + \log b_A, \quad E < E_A. \tag{4}$$

Combining the surface- and subsurface-source models yields the line shape to be expected from a semi-infinite homogeneous solid having a planar interface. It differs from the predictions of I in that following the characteristic elastic emission of an internal source the corresponding cascade can have both a slope parallel to the prethreshold slope and then change to a new slope; m_2. These effects are illustrated in Fig. 2.

In Sec. IV, experimental spectra will be examined in the $\log j(E)/\log(E)$ display mode to see the segmented cascade effects described here.

Delineation of surface-subsurface regions by an imaginary boundary at a depth $l_i(E)$ from the surface may seem to be rather restrictive, since "elastic" emission from below the surface is governed by an exponential attenuation term,

TABLE I. Distribution of isotropic emission from various thicknesses, $ml_i(E)$, of a homogeneous source, where $j_{A,m}$: emission, directed into $2\theta_A = \frac{1}{2}\pi$, which reaches surface elastically. $j_{0,m}$: emission, directed into $2\theta_A = \frac{1}{2}\pi$. $j_{c,m}$: emission, directed into $2\theta = \pi$, which cannot reach surface elastically. $j_{D,m}$: net half-space emission.

m	$j_{A,m}/j_{0,m}$	$\dfrac{j_{A,m}-j_{A,m-1}}{\sum_{m=1}^{6}(j_{A,m}-j_{A,m-1})}$	$j_{c,m}/j_{D,m}$	$j_{A,m}/j_{D,m}$
1	0.587	0.835	0.578	0.172
2	0.091	0.130	0.762	0.113
3	0.019	0.027	0.836	0.081
4	0.005	0.006	0.876	0.062
5	0.001	0.002	0.900	0.050

$\exp[-x/l_i(E)]$. Justification for this model is derived as follows. Consider a homogeneous source of isotropic emitters giving rise to a characteristic line such as an Auger line. Assume that the volume of active source is determined by the area A of the incident primary beam and by its depth of penetration ($\gg l_i$), and that the dimensions of the active source are small compared with the distance to the analyzer. We divide this active source into layers of thickness $l_i(E)$ and compute the fraction of the emission in each layer that contributes to the observed spectral line, subject to an exponential attenuation factor. The current reaching the surface elastically from a region of depth $x = ml_i(E)$ and directed into the analyzer aperture is given by

$$j(E,m) = vN(E)A\int_0^{ml_i} dx \int_1^{\cos\theta_A} d(\cos\theta) e^{-x/l_i\cos\theta}, \tag{5}$$

where θ_A is the half angle of a spherical-sector retarding potential analyzer. This current is to be compared with the net current emitted in the direction of the analyzer aperture, $j_0(E,m)$, where

$$j_0(E,m) = -vN(E)A\,ml_i(1-\cos\theta_A). \tag{6}$$

Hence, the fraction of the emission, originating in a layer of thickness ml_i beginning at the surface, directed into the analyzer aperature, which reaches the surface elastically is $j(E,m)/j_0(E,m)$, where

$$\frac{j(E,m)}{j_0(E,m)} = \frac{-1}{2m(1-\cos\theta_A)}\left\{m^2\left[e^{-\sqrt{2}m}\left(\frac{1}{2m^2}-\frac{1}{\sqrt{2}m}\right) - e^{-m}\left(\frac{1}{m^2}-\frac{1}{m}\right)\right.\right.$$
$$\left.\left. + \ln(\cos\theta_A) - \sum_{n=1}^{\infty}\frac{(-1)^n m^n}{nn!}\left(2^{n/2}-1\right)\right] - \sin^2\theta_a\right\}. \tag{7}$$

This equation has been evaluated with $\theta_A = \frac{1}{4}\pi$ to obtain the contribution from consecutive layers of thickness $l_i(E)$ with the results shown in Table I, column 3. It is evident from these data (see column 3 of Table I) that 84% of the elastic emission in a characteristic line originates in the surface-source region, $0 \le x \le l_i(E)$. Only 13% of the elastic emission derives from the next layer.

The isotropic emission from a homogeneous source can be divided into four catagories: (a) Emission initially directed toward the surface, which reaches the surface elastically in an aperture of solid angle $2\theta_A$; (b) emission initially outside the aperture cone of (a) which reaches the surface elastically; (c) emission directed toward the analyzer half space which does not reach the surface elastically; and (d) emission directed away from the analyzer half space. These categories of emission are illustrated in Fig. 4 where their relative magnitudes, for emission originating within the first $l_i(E)$ layer from the surface, are indicated (not to scale) by the variously marked areas of the isotropic emission circle. Obviously, 50% of the isotropic emission in a given layer belongs to catagory (d). The percentage of the emission in a given layer that belongs to catagory (c) can be computed from Eq. (5) as

$$\frac{j_c(E,m)}{j_D(D,m)} = 1 - \frac{1}{m}\int_0^m dm' \int_1^0 d(\cos\theta) e^{-m'/\cos\theta}. \tag{8}$$

Values from this calculation are given in the fourth column of Table I. Note that 58% of the outward emission in the first $l_i(E)$ layer does not reach the surface elastically. Also, of the outward emission from the first layer, only 17% can contribute to the characteristic Auger line (column 5 of Table I).

ISOTROPIC EMISSION FROM A HOMOGENEOUS SOURCE

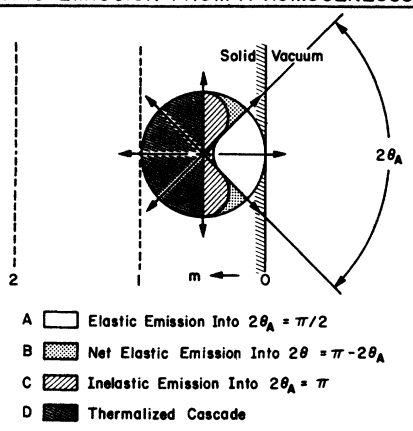

FIG. 4. Various components of isotropic emission from a homogeneous source are illustrated. The curved boundary within the isotropic emission circle, although not drawn to scale, serves to delineate the regions of elastic and inelastic emission directed toward the surface.

IV. LOG f(E)/LOG(E) SPECTRA

The features characteristic of internal sources are evident in all $\log j(E)/\log(E)$ displays examined

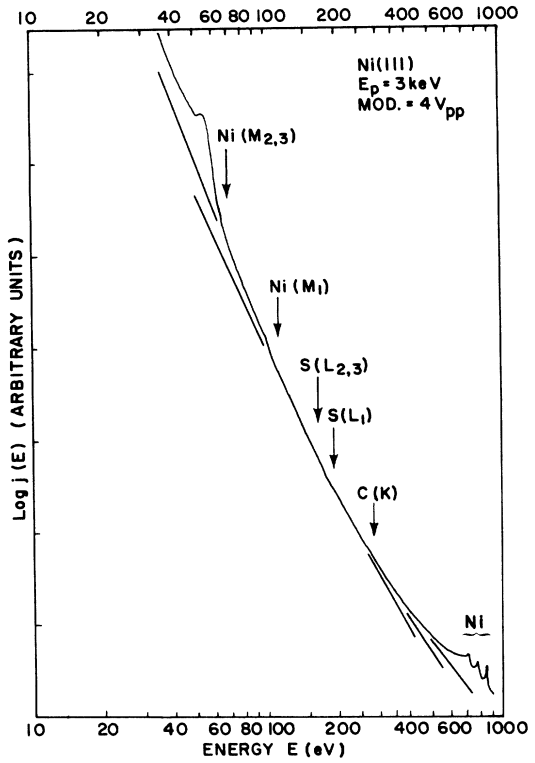

FIG. 5. Linearized cascade of a Ni(111) surface due to an incident primary beam of electrons of 3-keV energy. The high-energy Ni Auger electron peaks are labeled as a group. The binding energies of other electrons are marked with arrows.

thus far. Some of these are described below.

Figure 5 is a secondary-electron spectrum in the $\log j(E)/\log(E)$ display mode from a Ni(111) surface. As judged by the associated $dj(E)/dE$ spectrum, this specimen was designated Ni(111)—"clean." That is, there was no evidence of any Auger electron peaks other than Ni peaks in the $dj(E)/dE$ mode of display. The most obvious feature of the curve in Fig. 5 is the nearly linear nature of the spectrum from about 65–350 eV. On inspection, one notes marked changes in the slope at ~280 and 150 eV. At 100 and ~65 eV occur changes in slope and a discrete step to larger values of $\log j(E)$ with decreasing $\log(E)$. Each of these changes in slope and the steps correlate with the threshold of an Auger transition as indicated.

The segment of Fig. 5 below the 69-eV Ni Auger threshold has the characteristic of a composite homogeneous internal source extending throughout the surface and subsurface regions. It has a characteristic elastic emission peaked at 54 eV followed by a step having a slope parallel to the prethreshold ($E > 69$ eV) slope. This is the nature of a surface source. However, at lower energies, not shown in Fig. 5 the slope increases as expected due to the contribution from the subsurface region. This is evident for Ni as shown in Fig. 5 of I and for Al as seen in Fig. 8 of this paper.

The segment of Fig. 5 below the 113-eV Ni Auger threshold has also the characteristic of a composite source but with a greatly reduced elastic emission as compared with the Ni 55-eV peak. This is the result of rapid Koster-Cronig transitions causing potential Auger emission from the M_1 level to be shifted to the $M_{2,3}$ level of Ni. A similar effect is evident in Fig. 8 corresponding with the Al(L_1) → Al($L_{2,3}$) Koster-Cronig transition. The relative intensities of the (elastic) characteristic peaks and their associated (inelastic) steps between Ni(M_1) and Ni($M_{2,3}$) or between Al($L1$) and Al($L_{2,3}$) are consistent with the relative intensities to be expected from the escape-cone model. Namely, that ~$\frac{1}{6}$ of the surface source emission can contribute to the characteristic peak, while $\frac{1}{2}$ of the emission can contribute to the associated step. Thus steps may still be detectable when characteristic emission has become too weak.

Near $E = 165$ eV, another segmentation of the linearized cascade in Fig. 5 is evident. This one is characterized by the intersection of two linear segments having different slopes. There is no evidence of an elastic peak associated with this threshold nor a parallel step. This spectrum characterizes the surface after a cleaning process in which an original surface coverage of sulfur was removed by argon-ion sputtering. The cleaning procedure was continued until no evidence of the sulfur Auger peak could be seen in the derivative spectrum (nor any evidence of other contaminants). Upon examination in $\log j(E)/\log(E)$ display mode, however, the subsurface-type segmentation effect near 165 eV of Fig. 5 was found. We interpret this as evidence of subsurface sulfur. In the case of surface studies with nickel specimens it always has been possible to produce surface segregation of sulfur by heating. This result has been interpreted as surface segregation from a concentration of sulfur within the nickel specimen. The spectrum of Fig. 5 is typical of sputter cleaning of sulfur from nickel surfaces.

Note also in Fig. 5 that segmentation occurs near the carbon K threshold ($E = 284$ eV). Again, this segmentation has the properties of a subsurface source and is interpreted as such. Thus, although the surface of this specimen has been cleaned, as judged by the conventional criteria of derivative spectroscopy, the constituents that have been removed are still in evidence beneath the surface, as judged by this technique.

In Fig. 6 is shown the cascade spectrum of a Ni(110) surface in both the $\log j(E)$ vs $\log(E)$ and

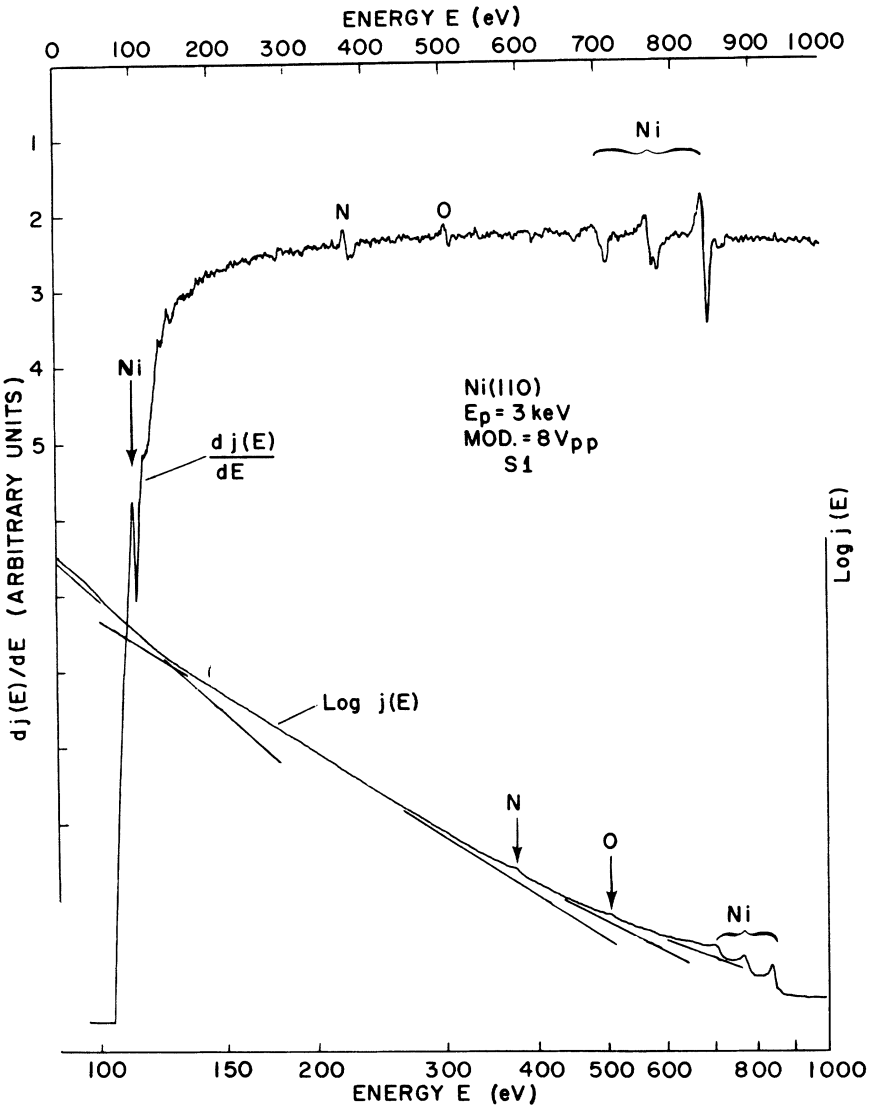

FIG. 6. Secondary-electron spectrum of a Ni(110) surface produced by a 3-keV beam of incident electrons. The upper curve is shown in the $d(E)/dE$ by E display mode while the lower curve is the same spectrum shown in the $\log j(E)$ display mode. The segmentation of the linearized display enhances detection of low-concentration constituents.

$dj(E)/dE$ vs E display modes. As is evident in these displays, the surface is not clean but exhibits both nitrogen and oxygen coverage. This specimen had been used to study various adsorbed oxygen line shapes to see if a strictly surface-type internal source could be produced. The resultant line shapes seemed to possess more the characteristic of a composite source than a surface source indicating that oxygen diffused readily to depths below $l_i(E \sim 500$ eV). Since nitrogen does not adsorb on clean nickel but can be made present in the surface by ion bombardment using nitrogen ions it was decided to compare the resultant cascade segmentation associated with nitrogen. In this case, it is expected that the nitrogen is entrained in the surface region with weak bonding, but does not exist on the surface as an adsorbate. Therefore, its line shape would be similar to a composite source, but (perhaps) with a weak subsurface contribution. As can be seen in Fig. 6 the nitrogen and oxygen segments of the cascade have well developed steps with a long range of parallel slope before the larger slope develops. They have also characteristic elastic emission indicating that the relevant surface atoms can emit Auger electrons directly into the vacuum.

The change in slope below $E = 150$ eV is related to the sulfur $L_{2,3}$ threshold at 165 eV. It occurs at lower energy here than in Fig. 5 because with the spectrum of Fig. 6 the surface region has been depleted more of sulfur. In this figure, the log $j(E)$ scale has not been expanded for examining in detail the cascade near 150 eV. However, from the upper curve it is evident that a step derivative

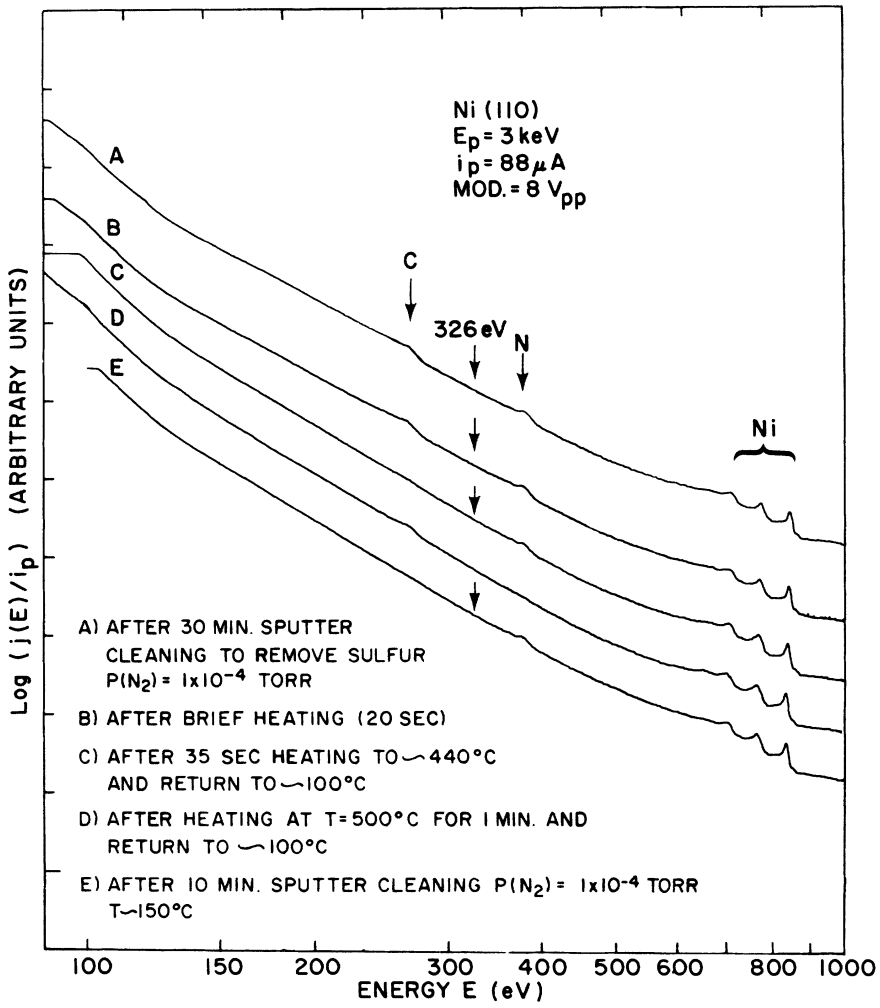

FIG. 7. Comparison of linearized cascade spectra from a Ni(110) surface bombarded by 3-keV electrons. These spectra were divided continuously by the beam-current intensity during recording to compensate for any beam current fluctuations. Surface composition changes between these spectra were produced by heating and by nitrogen-ion sputtering, (see text).

occurs near 150 eV where the sulfur Auger emission is expected.

In Fig. 7 several secondary-electron spectra are shown for a Ni(110) surface. Unlike the other spectra shown in this paper, these were obtained by dividing $j(E)$ by i_p before taking the logarithm. This was done as a check on the possibility of lineshape fluctuations associated with beam-current instabilities. Division was performed with an analog divider (PAR 230).

The Auger electron peaks of N and C are evident in Fig. 7 curve A in addition to the usual Ni peaks. Both of these peaks are characterized by a localized peak below the Auger transition threshold followed by a linear cascade toward lower energies. The cascade below the N peak is first a parallel step and then develops a second slope beginning near the energy marked by an arrow ($E \sim 326$ eV).

In these experiments, (curves A–E) it was of interest to try to produce a distributed source of nitrogen. Thus the ion-bombardment phase was conducted for longer periods than might otherwise be needed. Then, to check the result, the specimen was given a brief heating to see if the nitrogen would be lost from the surface. Curve B of Fig. 7 is an example of the result of a 20 sec heating ($T \sim 200\,^{\circ}$C)—a test for physisorption—that produced no strong changes in the original surface, curve A. In curve C is shown the result of heating the (b) surface condition for 35 sec in which time the temperature of the specimen rose to ~440 °C. Although somewhat diminished, the N peak still is evident but the C peak essentially has vanished. There now results a linear cascade extending from the N peak down to $E \sim 125$ eV. Note[5] that in the broad linear range around 200 eV that curve C has a greater slope than do curves A and B. This will be discussed below under carbon attenuation effects. Next the specimen was heated at ~500 °C for a period of 1 min. As shown in curve D, this

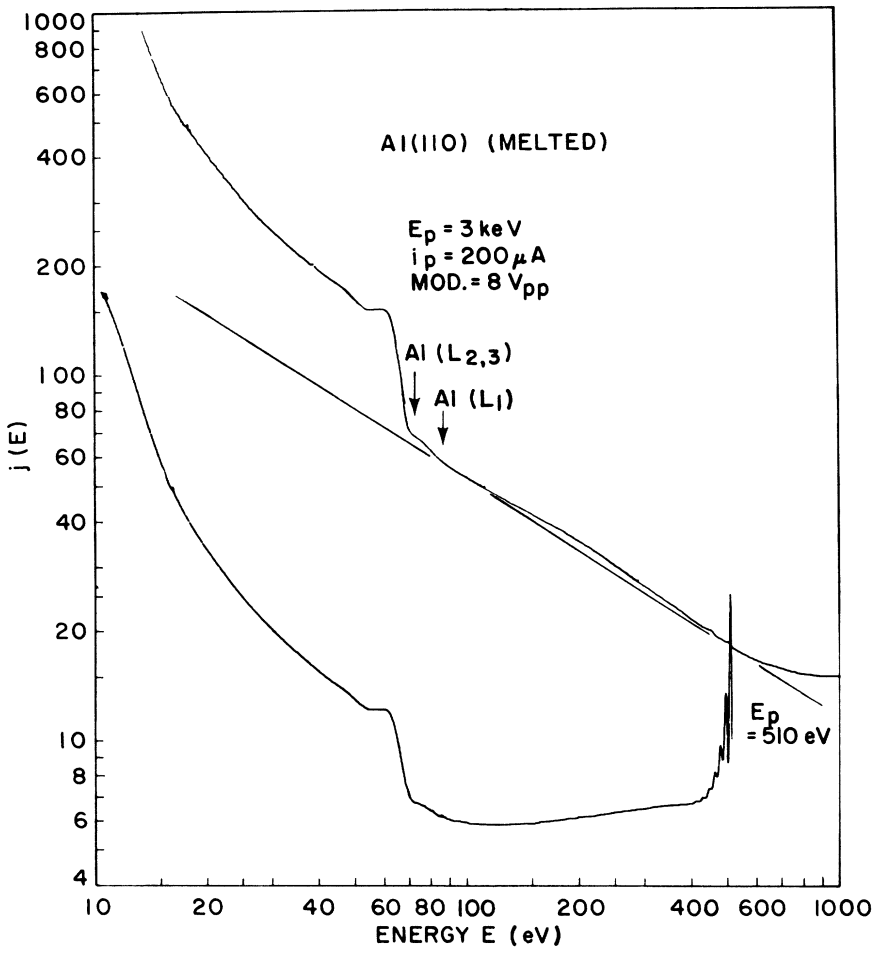

FIG. 8. Secondary-electron spectra from an aluminum surface (originally of (110) orientation but melted and resolidified *in situ*) subjected to a 3-keV beam of electrons in the upper curve and a 510-eV beam of electrons in the lower curve. Both curves are shown in the $\log j(E)/\log(E)$ display mode. The upper curve was made with an incident beam of low angle while the lower curve was made with a normally incident primary beam. The L_1 and $L_{2,3}$ binding energies of Al also are indicated.

caused the disappearance of the N peak, but not the break in the cascade at the nitrogen peak. It also permitted a reasonable coverage of surface carbon to develop. Finally, the specimen was bombarded again with nitrogen ions. The intent in this case was to sputter the surface clean of surface carbon and to produce surface nitrogen. The results of 10-min N-ion bombardment are shown in curve E. Note that the C peak has been removed but not the cascade break at the C peak. Also, the reappearance of the N peak is evident, with its linear-cascade tail.

The secondary electron cascade associated with a 3-keV primary beam incident on an aluminum specimen is shown in the upper part of Fig. 8. The lower curve is the secondary-electron spectrum associated with a 510-eV incident primary beam. In the upper curve is seen an almost linear-cascade extending from $E \sim 600$ to $E \sim 85$ eV and a short linear segment below the Auger peak at 60 eV ($28 < E < 40$ eV).

When first introduced into the vacuum chamber of the spectrometer this specimen exhibited a very large Auger oxygen peak. In the region of $\log j(E)/\log(E)$ below the O peak ($100 < E < 500$ eV) the curve exhibited a large, broad bowed shape and gave no indication of a linear trend. It was suspected that this was related to an extensively distributed source of oxygen commensurate with an oxide layer and its associated attenuation (similar to large carbon coverage). Hence, argon-ion sputtering was used to clean the surface of oxygen. The sputtering was continued until no trace of an 0 peak was detectable in the $dj(E)/dE$ mode. Then, upon investigating the $\log j(E)/\log(E)$ mode the results shown in Fig. 8 (upper curve) were found. Namely, that two barely visible peaks remain, at 510 and 455 eV (a faint trace of antimony), and the broad bowed shape had been reduced to an almost linear plot.

Along with the faint peak at 510 eV, the vestiges of the broad bowed shape are taken as evidence of remnants of a distributed oxygen source. However, relating the broad bow-shaped feature,

which extends down to $E \sim 110$ eV, to an internal source at 510 eV requires some justification. Although an external source at E_p is not exactly comparable to an internal source at E_p, for reasons discussed above, the complete secondary spectrum of an external source having $E_p = 510$ eV was examined. This is shown also in Fig. 8. The lower spectrum ($E_p = 510$ eV) was made with a normally incident primary beam while the upper spectrum was made with a glancing incidence beam. The lower spectrum shows multiple (~ 6) plasmon loss peaks adjacent to the elastic peak. The purpose of this comparison is to demonstrate that the excitation of the system by primaries of 510-eV energy produces a broad bow-shaped secondary region due to multiple scattering that reaches a minimum near 100 eV. This, being so similar to the bow-shaped region in the upper curve, is grounds for inferring that most of the nonlinear portion of the O section in the upper spectrum is due to Auger emission by internal oxygen which is subject to multiple scattering before escaping at the surface.

V. DISCUSSION AND CONCLUSIONS

In general, multiple internal sources increase the frequency of segmenting of the linearized cascade according to the number of sources. Each segment can be accompanied by an offset (a step) and a change in slope, depending on the type of internal source. Thus, in the absence of attenuation effects (e.g., curvature due to carbon) the segmented cascade will have increasing intensities with increasing slopes as energy is decreased. However, the net effect is that the more complex the surface being investigated, in terms of numbers of active internal sources, the more difficult it will become to observe linear segments in the $\log j(E)/\log(E)$ display mode.

According to the hypothesis of this paper, two slopes are needed to characterize segmentation of the linearized cascade by an internal source. The first is evident as a step for which the prethreshold slope is repeated below the threshold with a finite offset. The second is a larger slope than the prethreshold slope which, in the absence of a surface source, may join the parallel step near the threshold. Predominance of the first, the parallel step, is taken as characteristic of a surface source.

The basis for the line-shape distinction hypothesis is a phenomenological theory related to emission directly, or almost directly, into the vacuum. The source volume for direct emission into the vacuum has been described in terms of an emission cone. Isotropic emission from a surface source can be coupled directly to the vacuum from within this cone. Also, at least half of this isotropic emission becomes thermalized adequately so as to contribute to a step in the cascade. The line-shape effects associated with internal sources at or near the surface can be rather intense as compared with the overall cascade that develops from an external source. The latter begins with secondaries excited with momenta perpendicular to the direction of the primary. These then must scatter and diffuse until they reach the surface. They consequently are attenuated much more than the corresponding emission from surface sources. Consideration of the escape-cone volume can have a significant bearing on the interpretation of relative peak intensities.

It has been demonstrated that the remnants of Auger emission from M_1 and L_1 core vacancies, which are almost completely preempted by Koster-Cronig transitions, are made evident in the $\log j(E)/\log(E)$ display mode.

Finally, these line-shape effects in the linearized cascade demonstrate the synthesis of the observed spectrum. Thus, it follows that analysis of the segmented cascade offers a systematic approach to recovery of particular line-shape components.

ACKNOWLEDGMENTS

The author is grateful for the excellent assistance of C. Kukla in all phases of this work, and to L. C. Davis, W. Winterbottom, and C. Eagen for helpful discussions.

[1]The current leaving the surface with kinetic energy E is designated as $j(E)$, it is the free-space observable in these experiments. In other Auger-electron-spectroscopy literature $N(E)$ is used for this purpose. However, we choose to use the conventional notation of $N(E)$ for the electron distribution function and $j(E)$ for the current (see also Ref. 8 in I).

[2]P. A. Wolff, Phys. Rev. 95, 56 (1954).

[3]A. J. Bennett and L. M. Roth, Phys. Rev. B 5, 4309 (1972).

[4]A. J. Dekker, *Solid State Physics* (Prentice-Hall, Englewood Cliffs, N.J., 1960), Chap. 17.

[5]It is difficult to observe some of the breaks and slope changes described here when viewing the reduced graphs in this paper. It may be helpful to place a straight edge on these graphs to see the various features. In particular, parallel steps are most evident when a straight edge is placed on the linear part of the cascade to the high-energy side of an Auger threshold to aid comparison with the Auger emission toward the low-energy side. The graphs in Figs. 6–8 are photographic reproductions of the original 10-in. $\times$15-in. xy-recorder traces. The graph of Fig. 5 was first traced by hand to produce a wider line for subsequent reproduction.

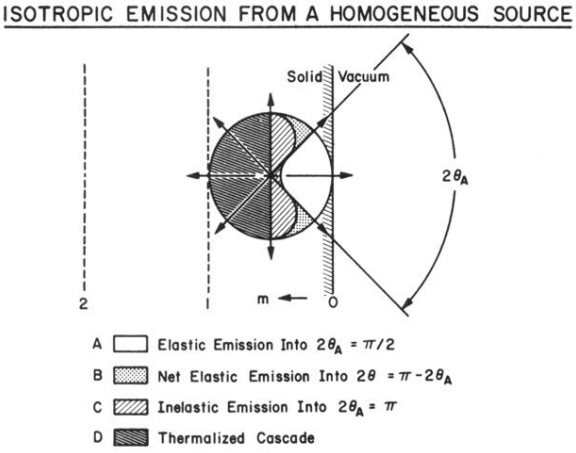

FIG. 4. Various components of isotropic emission from a homogeneous source are illustrated. The curved boundary within the isotropic emission circle, although not drawn to scale, serves to delineate the regions of elastic and inelastic emission directed toward the surface.